Draft version January 25, 2016
Preprint typeset using LaTeX style emulateapj v. 5/2/11

arXiv:1601.05808v1 [astro-ph.HE] 21 Jan 2016

TRANSPORT AND MIXING OF r-PROCESS ELEMENTS IN NEUTRON STAR BINARY MERGER BLAST WAVES

Gabriela Montes[1,2], Enrico Ramirez-Ruiz[1,2,3], Jill Naiman[2], Sijing Shen[4] and William H. Lee[5]

Draft version January 25, 2016

ABSTRACT

The r-process nuclei are robustly synthesized in the material ejected during a neutron star binary merger (NSBM), as tidal torques transport angular momentum and energy through the outer Lagrange point in the form of a vast tidal tail. If NSBM are indeed solely responsible for the solar system r-process abundances, a galaxy like our own would require to host a few NSBM per million years, with each event ejecting, on average, about $5 \times 10^{-2} M_{\odot}$ of r-process material. Because the ejecta velocities in the tidal tail are significantly larger than in ordinary supernovae, NSBM deposit a comparable amount of energy into the interstellar medium (ISM). In contrast to extensive efforts studying spherical models for supernova remnant evolution, calculations quantifying the impact of NSBM ejecta in the ISM have been lacking. To better understand their evolution in a cosmological context, we perform a suite of three-dimensional hydrodynamic simulations with optically-thin radiative cooling of isolated NSBM ejecta expanding in environments with conditions adopted from Milky Way-like galaxy simulations. Although the remnant morphology is highly complex at early times, the subsequent radiative evolution that results from thermal instability in atomic gas is remarkably similar to that of a standard supernova blast wave. This implies that sub-resolution supernova feedback models can be used in galaxy-scale simulations that are unable to resolve the key evolutionary phases of NSBM blast waves. Among other quantities, we examine the radius, time, mass and kinetic energy content of the NSBM remnant at shell formation as well as the momentum injected to the ISM. We find that the shell formation epoch is attained when the swept-up mass is about 10^3 $M_{\odot}$, at this point the mass fraction of r-process material is drastically enhanced up to two orders of magnitude in relation to a solar metallicity ISM.

Subject headings: hydrodynamics—nucleosynthesis, abundances—shock waves—stars: neutron—galaxies: ISM—ISM: supernova remnants

1. INTRODUCTION

The specific physical conditions and nuclear physics pathways required for the r-process were originally identified in the pioneering work by Burbidge et al. (1957). But the particular astrophysical site remains open to more than one interpretation (Sneden et al. 2008). Early work on the subject identified both type II supernovae (Woosley et al. 1994; Takahashi et al. 1994) and neutron-star binary mergers (NSBMs; Lattimer et al. 1977; Freiburghaus et al. 1999) as likely candidate events to hold r-process. NSBMs are significantly much rarer than type II supernovae (e.g. Argast et al. 2004) and take place far from their birth places, reaching distance up to a few Mpc from their host halo (e.g. Kelley et al. 2010). The two mechanisms synthesize different quantities of r-process material, about 10^{-5} $M_{\odot}$ and 10^{-2} $M_{\odot}$ for each type II supernovae and NSBM, respectively (e.g. Cowan & Thielemann 2004). These differences should give rise to clear signatures in the enrichment pattern of r-process elements in galaxies and may ultimately help constrain the dominant production mechanism (Shen et al. 2015).

With many difficulties getting the necessary conditions to produce the r-process in type II supernova winds (Qian & Woosley 1996; Takahashi et al. 1994) , the NSBM model has recently been extensively studied and shown to be a viable alternative. The r-process nuclei have been found to be robustly synthesized (Metzger et al. 2010; Roberts et al. 2011; Korobkin et al. 2012; Bauswein et al. 2013; Grossman et al. 2014; Ramirez-Ruiz et al. 2015; Goriely et al. 2015; Mendoza-Temis et al. 2015) and the predicted galactic enrichment history of NSBMs is consistent with the abundance patterns observed in halo stars (Shen et al. 2015; Tsujimoto & Shigeyama 2014; van de Voort et al. 2015; Vangioni et al. 2016). This suggests that the injection of r-process material by NSBMs has been operating in a fairly robust manner over long periods of time in galactic history, while the resultant chemical abundance dispersions in r-process elements such as Eu suggests an early, chemically unmixed and inhomogeneous early Milky Way galaxy. At later times, these localized inhomogeneities would fade out as more events happen and r-process products are given more time to be transported and mixed throughout the galaxy.

An accurate treatment of the evolution of the ejecta in NSBMs is thus crucial not only for models of electromagnetic transients (Nakar & Piran 2011; Rosswog

gmontes@ucsc.edu
[1] Department of Astronomy and Astrophysics, University of California, Santa Cruz, CA 95064
[2] Harvard-Smithsonian Center for Astrophysics, ITC, 60 Garden Street, Cambridge, MA 02138, USA
[3] Radcliffe Fellow
[4] Kavli Institute for Cosmology and Institute of Astronomy, University of Cambridge, Madingley Road, Cambridge CB3 0HA, UK
[5] Instituto de Astronomía, Universidad Nacional Autónoma de México, A. P. 70-264 04510 D. F. Mexico

et al. 2014; Kelley et al. 2013; Metzger & Berger 2012) following coalescence but also for models of r-process enrichment in galaxies. In contrast to the extensive efforts developing models for supernova remnant evolution, (Cox & Smith 1974; McKee & Ostriker 1977; Blondin et al. 1998; Joung & Mac Low 2006; Martizzi et al. 2015; Kim & Ostriker 2015) studies quantifying the impact of NSBM remnants in a cosmological context have not been carried out. The efficacy of transport and mixing of r-process in NSBM remnants has not been properly quantified mainly due to the highly inhomogeneous initial conditions and the excessive radiative losses expected during the shock propagation.

In this paper, we present the results of a series of controlled three-dimensional hydrodynamic simulations of NSBM remnants. To calculate the ejected mass and initial structure of the tidal tails, we make use of three-dimensional smoothed particle hydrodynamics simulations (Roberts et al. 2011) of NSBMs (Section 2.1). The resultant homologous structure of the tidal tail is then mapped into an adaptive mesh refinement (AMR) simulation with optically-thin radiative cooling (Section 2.2). Our goal is to understand the evolution of single NSBM remnants, which is quantified in Section 3, and how it might depend on the properties of the surrounding medium, which are derived using a cosmological simulation of the formation of the Milky Way (Section 2.3). Our simulations of isolated NSBMs are used to construct sub-resolution prescriptions for galaxy-scale simulations with inadequate resolution to properly define the the cooling radius of NSBM blast waves. Discussion of the results as well as detail comparisons with studies from spherical models are presented in Section 4.

2. METHODS

2.1. *Initial Conditions*

Tidal tails are a common feature formed during mergers and collisions between compact objects. These are typically a few thousand kilometers in size by the end of the merger event in the case of neutron star disruptions by black holes and NSBMs (Lee & Ramirez-Ruiz 2007; Faber & Rasio 2012). Some small fraction of the material ($10^{-3}-10^{-2} M_{\odot}$) in the tails is actually unbound and will escape to the surrounding medium. The exact mass and structure (density and velocity distribution) of the ejected material depends on the mass ratio and details of the equation of state (EoS; e.g. Roberts et al. 2011)

To calculate the density and velocity structure of the unbound tidal tails we use a similar method to the one described by Roberts et al. (2011). We use three-dimensional smoothed particle hydrodynamics (SPH) simulations (Lee & Ramirez-Ruiz 2007; Lee et al. 2010) to follow the merger of two neutron stars during which the geometry, densities, and timescales change violently (Rasio & Shapiro 1994; Lee 2000; Rosswog et al. 2003). As a representative example, we study the dynamics of the $M_{\rm r} = 0.05 M_{\odot}$ material ejected during a NSBM with mass ratio $q = M_2/M_1 = 0.88$ (Roberts et al. 2011). A hybrid EoS, similar to that implemented by Shibata et al. (2005), is used which combines the cold Friedman-Pandharipande-Skyrme nuclear EoS with an ideal gas component. Once the initial dynamical interaction is realized, the fluid elements in the unbound tails are verging on ballistic trajectories, moving primarily under the influence of the central mass potential. The hydrodynamical calculations are stopped only after the expansion of the unbound material becomes homologous. Figure 1 in Roberts et al. (2011) depicts the structure of the tidal tails at homology for a wide range of NSBMs. A clear progression is observed from equal mass tails formed in the $q = 1.0$ case to almost no secondary tail produced in the $q = 0.88$ case studied here.

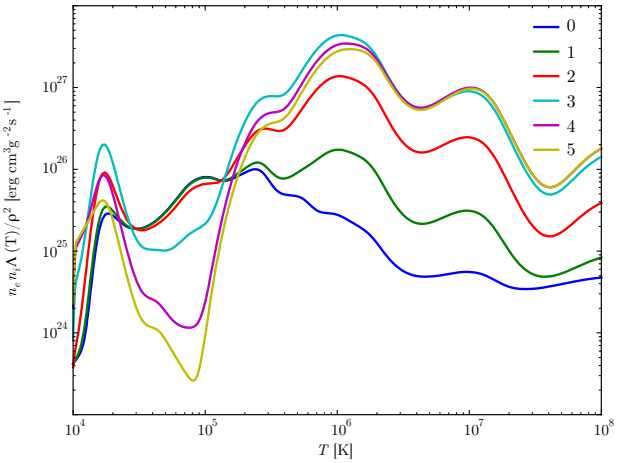

FIG. 1.— Cooling functions constructed using the ion-by-ion cooling efficiencies for low-density gas derived by Gnat & Ferland (2012) and assuming that the full radiative spectra of r-process material is similar to that of Fe. The computed cooling curves with enhanced metal abundances are plotted here as a function of the augmented Fe mass fraction $\xi_{\rm metal} = (\chi_{\rm Fe}/\chi_{\rm Fe,\odot}) = 10^0, 10^1, 10^2, 10^3, 10^4, 10^5$. The standard case of solar abundances is denoted here as $\log(\chi_{\rm Fe}/\chi_{\rm Fe,\odot}) = 0$. Once the cooling function is tabulated, the temperature variation within the expanding, cooling shocked layer in the NSBM remnant can be calculated.

2.2. *Hydrodynamical Evolution of NSBM Remnants*

Here we follow the expansion of the tidal tail produced by a NSBM with $q = 0.88$ in three dimensions with the parallel, adaptive-mesh, hydrodynamical code FLASH (Fryxell et al. 2000). We evolve the ideal fluid in three dimensional cartesian coordinates using a metallicity-dependent cooling function, which is constructed using the ion-by-ion cooling efficiencies for low-density gas derived by Gnat & Ferland (2012) for gas temperatures between 10^4 and 10^8 K. As it is generally adopted, we do not include metal fine structure transitions or molecular line cooling and so the cooling function is effectively truncated below $T \approx 10^4$ K.

Figure 1 shows the cooling function for an optically thin thermal plasma with solar abundances assuming collisional equilibrium (*blue* curve). The full radiative spectra of r-process material at the relevant densities and temperatures is not well known as complete atomic line lists for these heavy species are not available (Kasen et al. 2013; Tanaka et al. 2014; Lippuner & Roberts 2015). We therefore simply assume that the energy integral of the full radiative spectra of r-process material is similar to that of Fe. The computed cooling curves with enhanced Fe abundances are plotted in Figure 1. This assumption is, however, of no consequence at all as radiative losses begin to influence the NSBM remnant evolution

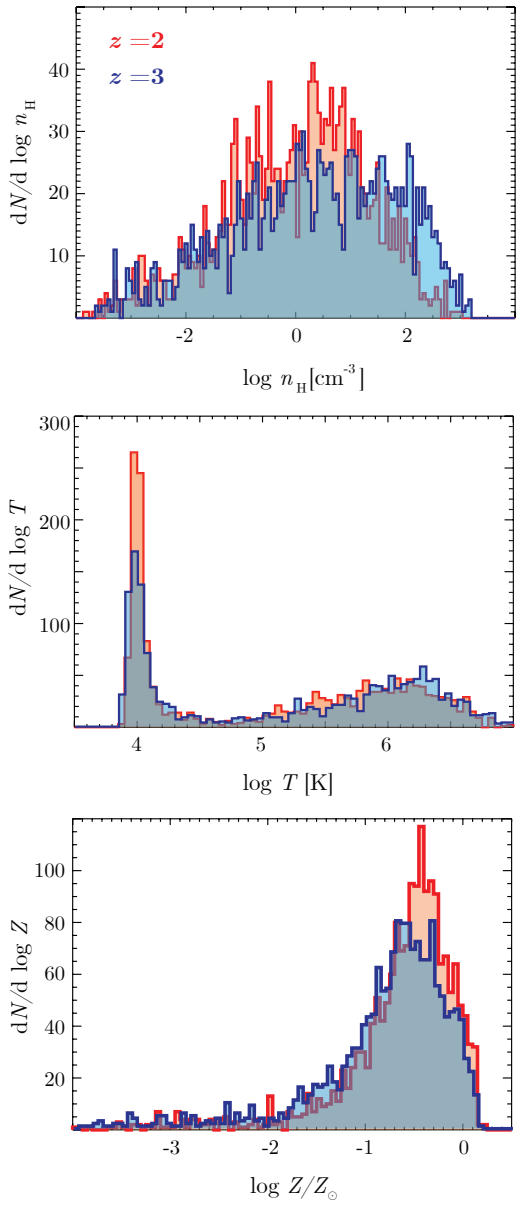

FIG. 2.— The gas density, temperature and metallicity at the NSBM injection sites in the Galaxy at redshifts $z = 2$ and 3, as derived from the Eris simulation (Shen et al. 2015; Guedes et al. 2011). The spatial distribution of NSBMs is assumed to broadly follow the stellar distribution of the host galaxy while the injection rate is derived using the Eris star formation rate convolved with a power-law delay-time distribution. Star We note that star formation in the simulation occurs when cold ($T < 3\times10^4$K) gas reaches the threshold density and as such cooling is effectively truncated.

only when the metal content is almost exclusively dominated by the swept up gas (see Section 3 for specifics). As such, the resulting evolution is quantitatively similar to that computed using solar abundances, but note that we have implemented metal enhanced cooling rates here for completeness.

2.3. *Properties of the Ambient Medium*

The evolution of a NSBM remnant depends on the character of the ambient medium. In Figure 2 we show the expected properties of the gas in and around the NSBM injection sites, derived using the cosmological zoom-in simulation Eris, which at redshift $z = 0$ is a close analog of the Milky Way (Guedes et al. 2011). The merger rate is inferred by convolving the star formation history with a standard delay-time distribution of mergers modeled by a power-law (Piran 1992; Kalogera et al. 2001; Shen et al. 2015). The resulting NSBM history in the simulation is shown in Figure 1 of Shen et al. (2015). The spatial distribution of NSBM mergers is then assumed to roughly follow the stellar distribution. Using these two key model ingredients, the number and location of NSBMs can then be estimated, which in turn can be used to infer the density, temperature and metallicity of the surrounding ambient gas (Figure 2). Motivated by this, we run three different types of simulations:

TABLE 1
INITIAL CONDITIONS AND AMBIENT MEDIUM PROPERTIES

Tidal Tail	NSBM with $q = 0.88$
M_r	5.8×10^{-2} $M_\odot$
E_k	3.58×10^{51} erg
ISM	
n_H	1 cm^{-3}
T	10^4 K
Z	$Z_\odot$
Rarefied	
n_H	10^{-4} cm^{-3}
T	10^6 K
Z	$Z_\odot$
Dense	
n_H	10^2 cm^{-3}
T	10^4 K
Z	$Z_\odot$

- isolated NSBM in a homogeneous ISM with $n_H = 1$ cm^{-3}, $T = 10^4$ K and $Z = Z_\odot$;
- isolated NSBM in a homogeneous, dense ISM with $n_H = 100$ cm^{-3}, $T = 10^4$ K and $Z = Z_\odot$;
- isolated NSBM in a homogeneous, rarefied ISM with $n_H = 10^{-4}$ cm^{-3}, $T = 10^6$ K and $Z = Z_\odot$.

The parameters of the different simulations are outlined in Table 1. For comparison, standard blast wave simulations initiated by injecting the same total energy in a spherical region are computed in order to determine how the evolution of a NSBM is initially altered by its non-uniform original structure. In all cases, we consider computational boxes filled with an ISM initially in pressure equilibrium and adopt a refinement scheme based on pressure and density gradients which refines around the expanding shock.

3. HYDRODYNAMICAL EVOLUTION OF NSBM REMNANTS

The evolution of an isolated NSBM remnant expanding into a uniform medium can be broadly characterized by the well-known evolutionary stages of a supernova remnant (SNR):

- the free expansion phase, during which the mass of the tidal ejecta is larger than the mass of the swept up ISM;
- the energy conserving phase, during which radiative losses are not important;

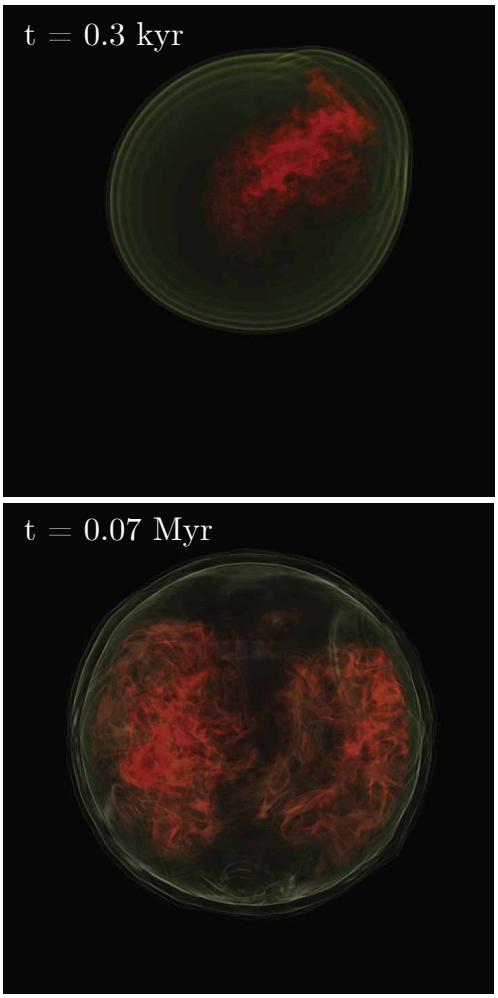

FIG. 3.— The evolution of a NSBM remnant expanding into a uniform ISM (fiducial run labelled *ISM* in Table 1). *Top panel*: Density contours (green) are plotted for 12 levels from $\log(\rho) = -23.4$ to -20.8 g cm-3. The mass fraction of metals in the ejecta, are denoted as $\chi_{\rm metal}$ and is assumed to have the cooling properties of Fe. The mass fraction of metals in the ejecta, denoted by $\chi_{\rm metal}$, is represented by surfaces (red) plotted with 16 levels from $\log(\chi_{\rm metal}) = -6$ to 0. The box size is 2.4 pc. *Bottom panel*: Density surfaces (green) are plotted for 12 levels from $\log(\rho) = -26$ to -20.7 g cm-3. $\chi_{\rm metal}$ contours (red) are plotted with 16 levels from $\log(\chi_{\rm metal}) = -6$ to 0. The box size is 20 pc. Total box size is 40 pc with 512×512 cells on the coarsest grid and 11 initial levels of refinement corresponding to a maximum resolution of 1.504×10^{16} cm. Levels of refinement are decreasing to reach a maximum level of eight with a maximum resolution of 1.203×10^{17} cm for the bottom snapshot.

- the cooling-modified pressure-driven snowplow phase, during which shell formation occurs;
- and the final momentum-conserving expansion phase.

However, differences in ejected mass and initial structure modifies the evolution of a NSBM remnant relative to that of a SNR, as illustrated in Figure 3 for our fiducial run (labelled *ISM* in Table 1). The top panel shows the evolution at time $t = 0.3$ kyr, long after the free expansion phase and during the energy conserving phase. The kinetic energy of the NSBM $q = 0.88$ tidal tail is 3.58×10^{51} erg. The ensuing strong blast wave converts much of this energy into thermal energy, which leads to lateral expansion[6]. As the NSBM remnant ages, the thermal energy is lost to radiative cooling, the shock slows down, and shell formation is established. The bottom panel in Figure 3 shows the effect of the blast wave propagation at time $t = 0.07$ Myr, before the onset of the remnant's cooling-modified snowplow phase.

The top panel of Figure 4 shows the evolution of the forward shock radius R with time t for the NSBM remnant case shown in Figure 3. For comparison, the evolution of a spherical blast wave with the same initial mass and energy is also shown together with the analytical Sedov-Taylor solution. For spherical simulations, R is identified by measuring spherically averaged profiles, while for the NSBM simulations we approximate R as the radius of the sphere enclosing 90% of the total energy (no significant difference in the measured radio was obtained from slightly different percentages). The radial temperature T and metal mass fraction $\chi_{\rm metal}$ profiles are then calculated by measuring the spherically averaged values of such quantities at R.

The initial configuration of the ejected tidal tail material is highly inhomogeneous, as can be seen in Figure 3, with shock expansion velocities being larger along the original orbital plane of the NS binary. As a result, the rate of ambient material swept up by the blast wave is reduced relative to the spherical case until lateral expansion becomes important. The Sedov-Taylor solution is an attractor and the NSBM remnant evolution slowly adjust to match this spherical, energy conserving solution. As shown in Figure 4, the NSBM remnant becomes radiative before matching the Sedov-Taylor solution, which increases the local cooling time and leads to a decrease in radiative losses when compared to the spherical case. Similar behavior is also seen in simulations of a NSBM remnant expanding into a dense ambient medium (Figure 5) and into a rarefied, hot external environment (Figure 6).

In a uniform medium, the shell formation epoch, which occurs when a SNR becomes radiative, is usually well characterized by the time the mass of swept up material attains $M_{\rm s} \approx 10^3 M_\odot$. Previous studies of SNRs expanding in a homogeneous ambient medium (Cioffi et al. 1988; Thornton et al. 1998) approximate the cooling radius as

$$R_{\rm s} \approx 14 \left(\frac{E_{\rm tot}}{10^{51}\ {\rm erg}}\right)^{2/7} \left(\frac{n_{\rm H}}{1\ {\rm cm}^{-3}}\right)^{-3/7} \left(\frac{Z}{Z_\odot}\right)^{-1/7} {\rm pc}. \quad (1)$$

Here we evaluate the radius $R_{\rm s}$, swept up mass $M_{\rm s}$, and kinetic energy $E_{\rm k}$ of the NSBM remnant at shell formation. The results for all simulations are given in Table 3. The radius, total remnant mass, and outward radial momentum at shell formation are similar to those obtain using spherical simulations and as such are close to the analytic estimates. Despite the initial differences in ejecta mass and geometry, our conclusions regarding shell formation and momentum injection in NSBM remnants are quite similar to those obtain for SNRs.

[6] Similar to the case of remnants arising from jet-driven supernova explosions (Ramirez-Ruiz & MacFadyen 2010; González-Casanova et al. 2014) or from the unbound debris of stars disrupted by massive black holes (Kasen & Ramirez-Ruiz 2010; Guillochon et al. 2015).

TABLE 2
PROPERTIES OF THE BLAST WAVE AT SHELL FORMATION

Simulation	R_s/pc	$M_s/M_\odot$	$E_{k,tail}/E_{k,sedov}$	¡ $\chi_r/\chi_{r,\odot}$¿	¡χ_{metal}¿
ISM	26.5	1.93×10^3	1.04	140.87	3.32×10^{-5}
Rarefied	471.72	1.09×10^3	1.04	243.90	5.73×10^{-5}
Dense	5.7	1.92×10^3	1.06	139.02	3.27×10^{-5}

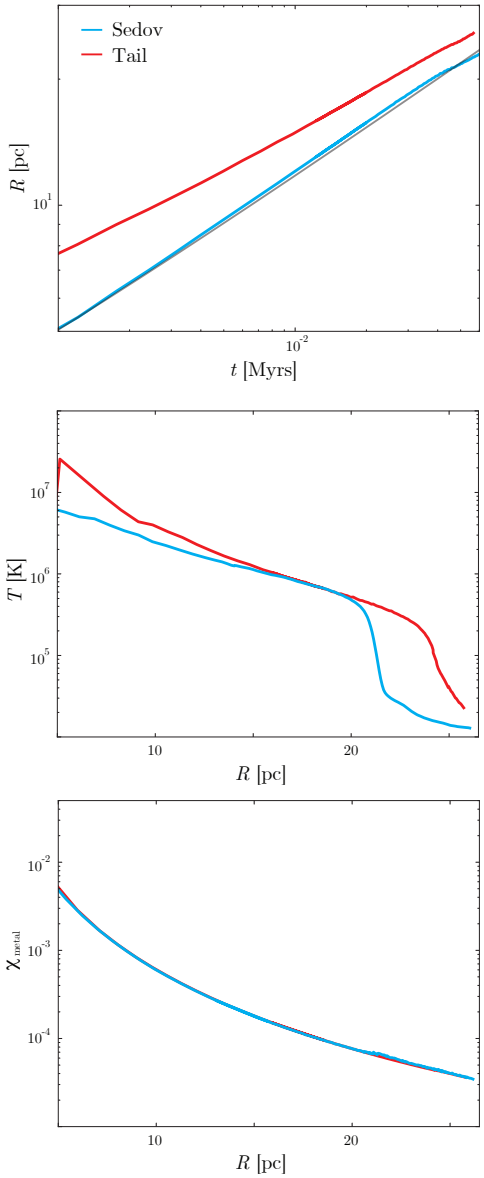

FIG. 4.— Evolution of the forward shock R with time t for the NSBM remnant case depicted in Figure 3 (labelled as *Tail*). The evolution of a spherical blast wave with identical energy and mass content, labelled as *Sedov*, is plotted for comparison. The analytical Sedov-Taylor solution $R(t)$ is shown as a grey line. Also shown are the temperature T and metal mass fraction χ_{metal} with R. The NSBM remnant propagates faster owing to the reduced rate of ambient mass sweeping, which is subsequently increased as the remnant becomes progressively more spherical. As a result, shell formation is delayed relative to the spherical case.

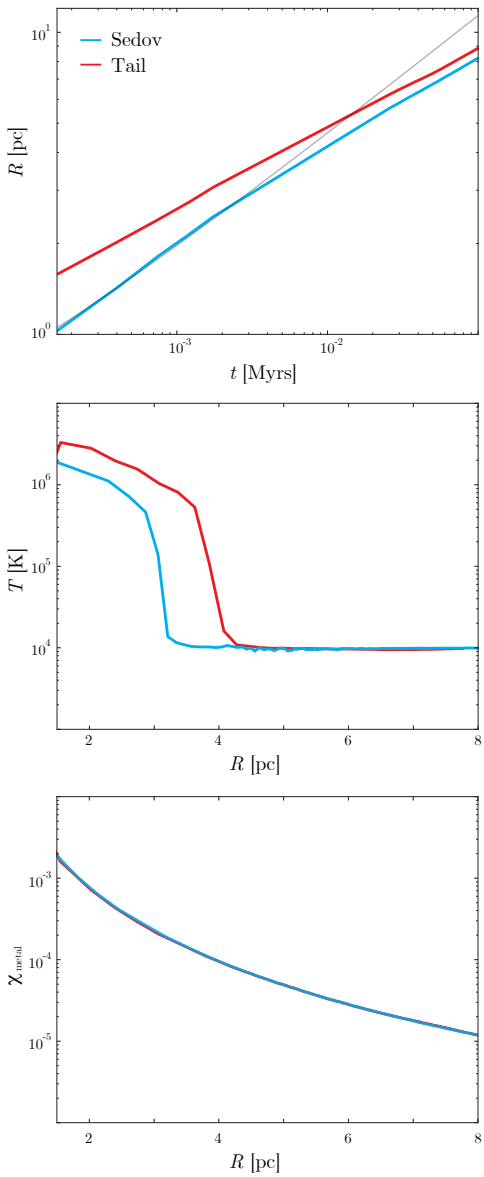

FIG. 5.— Similar to Figure 4 but for expansion into a dense ambient medium (labelled *Dense* in Table 1).

At the time of shell formation, the mass fraction χ_{metal} arising from metals ejected during the NSBM is about 5×10^{-5}. We thus only expect metal cooling from r-process material to influence the dynamics of NSBM remnants if they expand into an ambient medium with $Z \lesssim 10^{-3} Z_\odot$, under the assumption that the metal cooling function of r-process material is similar to that of Fe (Section 2.2). The r-process enrichment of the gas depends on how efficiently the metals are mixed with the ambient material swept up by the blast wave. At the time of shell formation, we find the mass fraction of r-process material in the NSBM remnant to be drastically enhanced in relation to solar metallicity to about

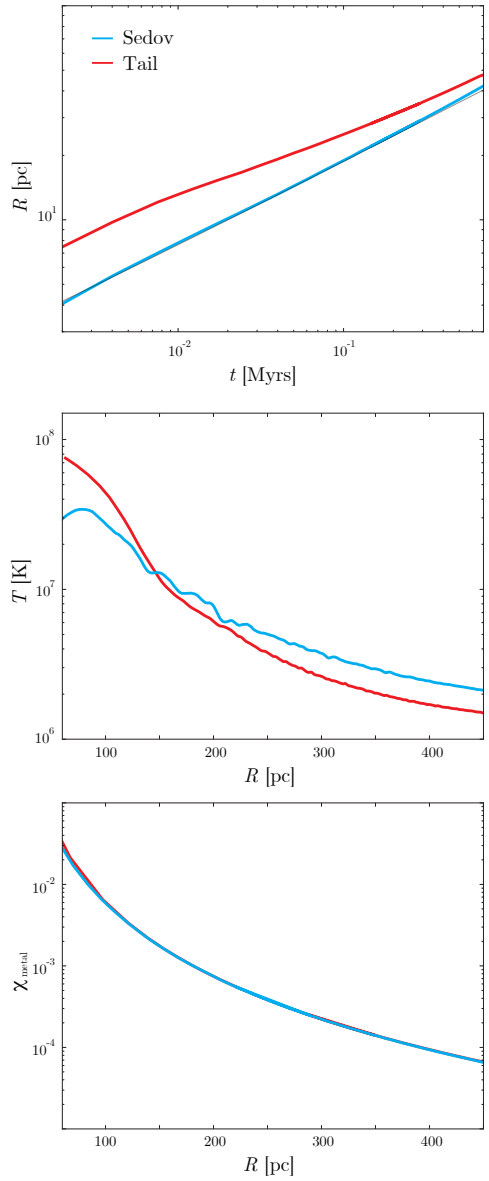

FIG. 6.— Similar to Figure 4 but for expansion into a rarefied and hot ambient medium (labelled *Rarefied* in Table 1).

$10^2\,(Z/Z_\odot)$.

4. DISCUSSION AND CONCLUSIONS

The importance of SNR evolution for detailed models of the ISM but also for models of galaxy evolution and chemical enrichment has been appreciated for decades. In recent years, it has become increasingly clear that an accurate treatment of NSBM remnant evolution is crucial not just for detailed models of electromagnetic transients (Nakar & Piran 2011; Rosswog et al. 2014; Kelley et al. 2013; Metzger & Berger 2012) but also for models of heavy element enrichment (Shen et al. 2015; Tsujimoto & Shigeyama 2014; van de Voort et al. 2015). NSBMs are thought to play a predominant role in creating (Metzger et al. 2010; Roberts et al. 2011; Korobkin et al. 2012; Bauswein et al. 2013; Grossman et al. 2014; Ramirez-Ruiz et al. 2015; Goriely et al. 2015; Vangioni et al. 2016) and dispersing r-process elements, yet modern cosmological simulations are still not able to resolve the expansion of SNRs. Motivated by this, we have perform a series of three-dimensional hydrodynamic simulations of isolated NSBM remnants expanding in environments with thermodynamical properties similar to those found in cosmological simulations (Section 2.3). Particularly important is the use of realistic merger simulations (Roberts et al. 2011) for constructing the initial conditions characterizing the structure of the ejected tidal debris (Section 2.2). We have centered our attention in particular on the evolution of NSBM remnants during the well-known stages that are commonly used to describe the evolution of SNRs.

- First, a free expansion phase is observed, during which the mass of the ejecta is larger than the mass of the swept up gas. This evolutionary phase is significantly shorter than that of a typical SNR due mainly to the low mass content of the ejecta ($5.8\times10^{-2}\ M_\odot$) and, to a lesser degree, the initial complex geometry.

- Secondly, an energy conserving phase takes place, during which radiative losses are negligible (Figure 3). During this phase the rate of mass swept up by the blast wave is reduced when compared to a standard SNR but is then subsequently increased as the NSBM remnant becomes progressively more spherical. However, radiative losses begin to influence the NSBM remnant evolution before it is accurately described by a standard spherical solution (Figure 4). In addition, the overall evolution takes slightly longer, with the cooling time reaching its critical value only when the shock has travelled a distance that is a few times larger than in the spherical case. This is observed in all simulations listed in Table 1.

- Thirdly, a pressure-driven snowplow phase sets in, during which radiative losses begin to influence the evolution of the NSBM remnant and shell formation is found to set in at a time when the swept up mass attains a value of $M_{\rm s}\approx10^3 M_\odot$, as it is commonly found in SNRs (Table 3). The radius, total swept-up mass, kinetic energy and outward radial momentum at shell formation for NSBM remnants, we conclude, are close to the standard estimates given for SNRs (Cox & Smith 1974; McKee & Ostriker 1977; Blondin et al. 1998; Joung & Mac Low 2006).

- Finally, during the momentum conserving phase, the evolution of a NSBM remnant is remarkably similar to that of a SNR. This implies that subresolution supernova feedback models (e.g. Martizzi et al. 2015; Kim & Ostriker 2015) can be accurately used in galaxy-scale simulations that are unable to resolve the early evolutionary stages of a NSBM remnant.

While our simulations of NSBM remnants have confirmed the similarities and highlighted the differences of the well-known evolutionary stages of SNRs, one of the key distinct processes affecting their structure is the contribution of r-process material to the cooling of the

swept-up material. As complete atomic line lists for these heavy species are not available (Kasen et al. 2013), we have thus simply assumed that the energy integral of the full radiative spectra of r-process material is similar to that of Fe. Under these conditions, we find that metal cooling from r-process material is not expected to influence the dynamics of NSBM remnants expanding into an ambient medium with $Z \gtrsim 10^{-3} Z_{\odot}$. The resulting NSBM remnant evolution in these environments should solely be determined by the metal cooling of the swept-up material. Yet, the mass fraction of r-process material at shell formation within the remnant is expected to be severely enhanced to about 2.5×10^4 $(Z/10^{-2} Z_{\odot})$, assuming a solar abundance ratio. In contrast, with a total r-process mass per supernova of $M_{\rm p} \approx 7.4 \times 10^{-5} M_{\odot}$ (Shen et al. 2015), we expect a local enhancement of only about 31.9 $(Z/10^{-2} Z_{\odot})$ when a Type II SNR attains shell formation.

Of particular relevance in this case are the heavy element composition of galactic halo stars with metallicity regime $10^{-3} Z_{\odot} \lesssim Z \lesssim 10^{-2} Z_{\odot}$, which have been found to have pure r-process products with a distribution that is characteristic of solar system matter but with a large star-to-star scatter in their r-process concentrations (Sneden et al. 2008). In some stars with $Z \approx 10^{-2} Z_{\odot}$, the r-process enrichment can be as large as 10^2, assuming a solar abundance ratio. The presence of r-process material in these stars with a distribution that is characteristic of solar abundance ratios illustrates that r-process enrichment has operated in a fairly robust manner, while their abundance dispersions further suggests that r-process production sites must be rare and locally very enhanced, as expected from NSBM enrichment (e.g. Shen et al. 2015). These localized inhomogeneities would then be smoothed out as more NSBMs take place and r-process material is given more time to be transported and mixed throughout the early Milky Way. Metal feedback from NSBM remnants is thus essential to understand the formation of r-process enhanced stars in galaxies. Despite the initial differences, our conclusions regarding the efficacy of the transport and mixing of r-process material by NSBM remnants in a cosmological context should be similar to that expected from single SNRs.

We thank R. Cooke, D. Kasen, E. Kirby and L. Roberts for insightful discussions and acknowledge financial support from the David and Lucile Packard Foundation, NSF (AST0847563) and UCMEXUS (CN-12-578). G. MONTES acknowledges to AAUW American Fellowship 2014-15. We gratefully acknowledge the hospitality of the Aspen Center for Physics, the Radcliffe Institute for Advanced Study and the the DARK Cosmology Center while completing this work.

REFERENCES

Argast, D., Samland, M., Thielemann, F.-K., & Qian, Y.-Z. 2004, A&A, 416, 997
Bauswein, A., Goriely, S., & Janka, H.-T. 2013, ApJ, 773, 78
Blondin, J. M., Wright, E. B., Borkowski, K. J., & Reynolds, S. P. 1998, ApJ, 500, 342
Burbidge, E. M., Burbidge, G. R., Fowler, W. A., & Hoyle, F. 1957, Reviews of Modern Physics, 29, 547
Cioffi, D. F., McKee, C. F., & Bertschinger, E. 1988, ApJ, 334, 252
Cowan, J. J., & Thielemann, F.-K. 2004, Physics Today, 57, 47
Cox, D. P., & Smith, B. W. 1974, ApJ, 189, L105
Faber, J. A., & Rasio, F. A. 2012, Living Reviews in Relativity, 15, 8
Freiburghaus, C., Rosswog, S., & Thielemann, F.-K. 1999, ApJ, 525, L121
Fryxell, B., Olson, K., Ricker, P., et al. 2000, ApJS, 131, 273
Gnat, O., & Ferland, G. J. 2012, ApJS, 199, 20
Guillochon, J., McCourt, M., Chen, X., Johnson, M. D., & Berger, E. 2015, arXiv:1509.08916
González-Casanova, D. F., De Colle, F., Ramirez-Ruiz, E., & Lopez, L. A. 2014, ApJ, 781, L26
Goriely, S., Bauswein, A., Just, O., Pllumbi, E., & Janka, H.-T. 2015, arXiv:1504.04377
Grossman, D., Korobkin, O., Rosswog, S., & Piran, T. 2014, MNRAS, 439, 757
Guedes, J., Callegari, S., Madau, P., & Mayer, L. 2011, ApJ, 742, 76
Joung, M. K. R., & Mac Low, M.-M. 2006, ApJ, 653, 1266
Kalogera, V., Narayan, R., Spergel, D. N., & Taylor, J. H. 2001, ApJ, 556, 340
Kasen, D., Badnell, N. R., & Barnes, J. 2013, ApJ, 774, 25
Kasen, D., & Ramirez-Ruiz, E. 2010, ApJ, 714, 155
Kelley, L. Z., Ramirez-Ruiz, E., Zemp, M., Diemand, J., & Mandel, I. 2010, ApJ, 725, L91
Kelley, L. Z., Mandel, I., & Ramirez-Ruiz, E. 2013, Phys. Rev. D, 87, 123004
Kim, C.-G., & Ostriker, E. C. 2015, ApJ, 802, 99
Korobkin, O., Rosswog, S., Arcones, A., & Winteler, C. 2012, MNRAS, 426, 1940
Lattimer, J. M., Mackie, F., Ravenhall, D. G., & Schramm, D. N. 1977, ApJ, 213, 225
Lee, W. H. 2000, MNRAS, 318, 606
Lee, W. H., Ramirez-Ruiz, E., & van de Ven, G. 2010, ApJ, 720, 953
Lee, W. H., & Ramirez-Ruiz, E. 2007, New Journal of Physics, 9, 17
Lippuner, J., & Roberts, L. F. 2015, arXiv:1508.03133
Martizzi, D., Faucher-Giguère, C.-A., & Quataert, E. 2015, MNRAS, 450, 504
McKee, C. F., & Ostriker, J. P. 1977, ApJ, 218, 148
Mendoza-Temis, J. d. J., Wu, M.-R., Langanke, K., et al. 2015, Phys. Rev. C, 92, 055805
Metzger, B. D., Martínez-Pinedo, G., Darbha, S., et al. 2010, MNRAS, 406, 2650
Metzger, B. D., & Berger, E. 2012, ApJ, 746, 48
Nakar, E., & Piran, T. 2011, Nature, 478, 82
Piran, T. 1992, ApJ, 389, L45
Qian, Y.-Z., & Woosley, S. E. 1996, ApJ, 471, 331
Ramirez-Ruiz, E., & MacFadyen, A. I. 2010, ApJ, 716, 1028
Ramirez-Ruiz, E., Trenti, M., MacLeod, M., et al. 2015, ApJ, 802, L22
Rasio, F. A., & Shapiro, S. L. 1994, ApJ, 432, 242
Roberts, L. F., Kasen, D., Lee, W. H., & Ramirez-Ruiz, E. 2011, ApJ, 736, L21
Rosswog, S., Ramirez-Ruiz, E., & Davies, M. B. 2003, MNRAS, 345, 1077
Rosswog, S., Korobkin, O., Arcones, A., Thielemann, F.-K., & Piran, T. 2014, MNRAS, 439, 744
Shen, S., Cooke, R. J., Ramirez-Ruiz, E., et al. 2015, ApJ, 807, 115
Shibata, M., Taniguchi, K., & Uryū, K. 2005, Phys. Rev. D, 71, 084021
Sneden C., Cowan J. J., Gallino R., 2008, ARA&A, 46, 241
Takahashi, K., Witti, J., & Janka, H.-T. 1994, A&A, 286, 857
Tanaka, M., Hotokezaka, K., Kyutoku, K., et al. 2014, ApJ, 780, 31
Thornton, K., Gaudlitz, M., Janka, H.-T., & Steinmetz, M. 1998, ApJ, 500, 95
Tsujimoto, T., & Shigeyama, T. 2014, ApJ, 795, L18
Woosley, S. E., Wilson, J. R., Mathews, G. J., Hoffman, R. D., & Meyer, B. S. 1994, ApJ, 433, 229

van de Voort, F., Quataert, E., Hopkins, P. F., Kereš, D., & Faucher-Giguère, C.-A. 2015 MNRAS, 447, 140
Vangioni, E., Goriely, S., Daigne, F., François, P., & Belczynski, K. 2016, MNRAS, 455, 17